Photoelectrochemical Reduction of *p*-Halonitrobenzenes

Richard G. Compton,* Robert A. W. Dryfe and Adrian C. Fisher
Physical Chemistry Laboratory, Oxford University, South Parks Road, Oxford, UK OX1 3QZ

A detailed and comparative mechanistic study of the photoelectrochemical dehalogenation of the four *p*-halonitrobenzenes, X-C_6H_4-NO_2 (X = F, Cl, Br, or I) in acetonitrile solution is reported. In the case of *p*-iodonitrobenzene, iodide loss is accomplished by electrochemical reduction alone. The formation of I^- is shown to take place *via* an ECE process with the ultimate generation of the radical anion of nitrobenzene. Dual photo- and electro-chemical activation of *p*-chloronitrobenzene and *p*-bromonitrobenzene leads to halide loss through a photo-ECE mechanism. This proceeds *via* absorption of light by the radical anions, $[X\text{-}C_6H_4\text{-}NO_2]^{\bullet -}$, which is followed by fragmentation forming the $^{\bullet}C_6H_4NO_2$ aryl radical. The latter is shown to react with the solvent system forming nitrobenzene which is further reduced at the electrode with the generation of $[C_6H_4\text{-}NO_2]^{\bullet -}$. The aryl radical is demonstrated to be able to undergo (partial) recombination with added Br^- or Cl^-. The effectiveness of different electronic transitions in the radical ions, $[X\text{-}C_6H_4\text{-}NO_2]^{\bullet -}$ (X = Br, Cl) towards dehalogenation are compared; both radical anions exhibit transitions centred near 330 and 470 nm in the near UV–VIS part of the spectrum. For the chloro-compound only the former band is effective in stimulating chloride release, whereas for the bromo-compound the excitation of either band causes bromide loss. The long wavelength band of the latter is quantified as being some 5.6 times more effective towards fragmentation on a per photon absorbed basis and this is rationalised using spin selection rules. No loss of fluoride from $[F\text{-}C_6N_4\text{-}NO_2]^{\bullet -}$ was observed at any wavelength in the visible region of the spectrum.

In a preliminary note[1] we have reported that the dual photo- and electro-chemical activation of *p*-chloronitrobenzene **1** and *p*-bromonitrobenzene **2** in acetonitrile solution leads to efficient dehalogenation through the expulsion of halide ion. Subsequently[2] a detailed mechanistic investigation of the electroreduction of the *p*-bromonitrobenzene system in the presence of light of wavelengths around 330 nm showed that the light was absorbed by the radical anion, $[Br\text{-}C_6H_4\text{-}NO_2]^{\bullet -}$, formed *via* the one-electron reduction of **2**. The photofragmentation of this ion radical was demonstrated to lead to the formation of the nitrobenzene radical anion, $[C_6H_4NO_2]^{\bullet -}$, *via* the following photo-ECE mechanism [eqns. (a)–(d)], where HS is the solvent

$$p\text{-}Br\text{-}C_6H_4\text{-}NO_2 + e^- \longrightarrow [p\text{-}Br\text{-}C_6H_4\text{-}NO_2]^{\bullet -} \quad (a)$$

$$[p\text{-}Br\text{-}C_6H_4\text{-}NO_2]^{\bullet -} + h\nu \longrightarrow Br^- + {}^{\bullet}C_6H_4NO_2 \quad (b)$$

$$^{\bullet}C_6H_4NO_2 + HS \longrightarrow C_6H_5NO_2 + S^{\bullet} \quad (c)$$

$$C_6H_5NO_2 + e^- \longrightarrow [C_6H_4NO_2]^{\bullet -} \quad (d)$$

system. The further reduction,

$$S^{\bullet} + e^- \longrightarrow S^- \quad (e)$$

was shown to be kinetically insignificant [eqn. (e)].[2]

In this paper we report a detailed and comparative mechanistic study of the photoelectrochemical reduction of all four *p*-halonitrobenzenes, X-C_6H_4-NO_2 where X = F **3**, Cl, Br or I **4**, with the aim of exploring first the generality of the dehalogenation process, and second, the relative effectiveness of different electronic transitions within the radical anions, $[X\text{-}C_6H_4\text{-}NO_2]^{\bullet -}$, in respect of inducing their photofragmentation. The latter effects are interpreted in terms of spin conservation rules applied to the fragmentation process.

Experimental

All standard photofragmentation voltammetry experiments were conducted using a platinum channel electrode made of optical quality synthetic silica to standard construction and dimensions.[3–5] Solution (volume) flow rates between 10^{-4} and 10^{-1} cm^3 s^{-1} were employed. Working electrodes were fabricated from Pt foils (purity of 99.95%, thickness 0.025 mm) of approximate size 4 mm × 4 mm, supplied by Goodfellow Advanced Materials. Precise electrode dimensions were determined using a travelling microscope. A saturated calomel reference electrode (SCE) was positioned in the flow system upstream, and a platinum gauze counter electrode located downstream, of the channel electrode. Electrochemical measurements were made using an Oxford Electrodes potentiostat modified to boost the counter electrode voltage (up to 200 V). Other methodological details were as described previously.[3–5] Irradiation was provided by one of two sources: (*i*) a Wotan XBO 900 W/2 xenon arc lamp used in conjunction with a Jarrell-Ash 82-410 grating monochromator (maximum incident power 2.0 mW cm^{-2}), an arrangement which permitted variable light intensity measurements through attentuation of the beam as described previously[3] or (*ii*) an Omnichrome continuous wave 3112XM He–Cd source (Omnichrome, Chino, California) which gave light of wavelength 325 nm at 20 mW absolute power and a minimum beam diameter of 1.6 mm. The laser was used in conjunction with a beam expander (Optics for Research, Caldwell, New Jersey) which gave a 25-fold increase in the beam area and a radiative power of 55 mW cm^{-2}.

Simultaneous photoelectrochemical EPR experiments used a channel flow cell carefully positioned in the TE_{102} cavity of an X-band (9.0–10.0 GHz) Bruker ER200D spectrometer as previously described.[6] UV–VIS measurements of electrogenerated species were made using an optically transparent thin-layer electrode (OTTLE)[7] in combination with a Perkin-Elmer Lambda-5 spectrometer.

Experiments were performed using solutions of *p*-halonitrobenzene (*ca.* 10^{-4}–10^{-3} mol dm^{-3}) in dried[3] acetonitrile (Fisons, dried, distilled) solution containing 0.1 mol dm^{-3} (recrystallised)

tetrabutylammonium perchlorate (TBAP) (Kodak) as supporting electrolyte. Solutions were purged of oxygen by outgassing with prepurified argon prior to electrolysis.

TMPD, nitrobenzene, *p*-iodonitrobenzene, *p*-bromonitrobenzene, *p*-chloronitrobenzene and *p*-fluoronitrobenzene were used as received from Aldrich (>99%). Tetrabutylammonium bromide (TBAB) was purchased from Fluka and tetrabutylammonium chloride (TBAC) from Janssen.

Results and Discussion

We report first the experimental results obtained for each of the four substrates and nitrobenzene in the absence of light before considering their photoelectrochemical behaviour. In all cases, the observed voltammetry is consistent with literature reports[8] except where discussed.

Dark Electrochemistry.—p-*Fluoronitrobenzene.* A reversible one-electron reduction in acetonitrile–0.1 mol dm^{-3} TBAP was observed with a halfwave potential of −1.10 V (*vs.* SCE) as evidenced by hydrodynamic voltammograms measured at a Pt channel electrode. Measurement of the steady-state transport limited current as a function of the electrolyte flow rate revealed a cube root dependence in accord with the Levich equation for a simple one-electron reduction, where F is

$$I_{lim} = 0.925\,F[C]_{bulk}wx_\theta^{2/3}D^{2/3}\{V_f/h^2d\}^{1/3} \quad (1)$$

the Faraday constant, $[C]_{bulk}$ the bulk concentration of the electroactive species, D its diffusion coefficient, $2h$ the depth of the channel, x_θ the electrode length, w the electrode width and d the channel width.[9] Application of eqn. (1) gave a value of 2.15×10^{-5} cm^2 s^{-1} for the diffusion coefficient of **3**.

The nature of the electrode process in the absence of light was confirmed as a one-electron reduction leading to the kinetically stable radical anion of **3**, by means of *in situ* electrochemical EPR experiments in which the channel electrode was located in the TE_{102} cavity of an X-band spectrometer and spectra recorded simultaneously with electrolysis. Fig. 1 shows the EPR spectrum derived from the electrolysis of **3** and attributable to the radical anion $[F\text{-}C_6H_4\text{-}NO_2]^{\bullet -}$.[10] We have shown elsewhere that if the EPR visible species is the sole electrolysis product, and that it is kinetically stable, then the intensity of the EPR signal, S, is related to the electrode current (I) and flow rate by eqn. (2).[11]

$$S \propto I/V_f^{2/3} \quad (2)$$

Experimental measurements of the EPR signal intensity made as a function of flow rate and electrode current were found to be in quantitative agreement with eqn. (2)—plots of $\log(S/I)$ against $\log(V_f)$ were found to have a slope of (-0.67 ± 0.01). This indicates that the radical anion, $[p\text{-}F\text{-}C_6H_4\text{-}NO_2]^{\bullet -}$, has a lifetime of at least several seconds.

The UV–VIS spectrum of $[p\text{-}F\text{-}C_6H_4\text{-}NO_2]^{\bullet -}$ shown in Fig. 2 was recorded using an OTTLE.[7] The spectrum of the parent compound is shown for comparison. The radical anion spectrum shows bands at $\lambda_{max} = 310$ ($\varepsilon = 7270$) and 440 nm (1210 dm^3 mol^{-1} cm^{-1}). In contrast the parent molecule shows a longest wavelength absorption band at 255 nm (8790 dm^3 mol^{-1} cm^{-1}) with negligible absorption above 300 nm.

p-*Chloronitrobenzene.* A reversible one-electron reduction in acetonitrile–0.1 mol dm^{-3} TBAP was seen with a halfwave potential of −1.05 V (*vs.* SCE) on the basis of channel electrode

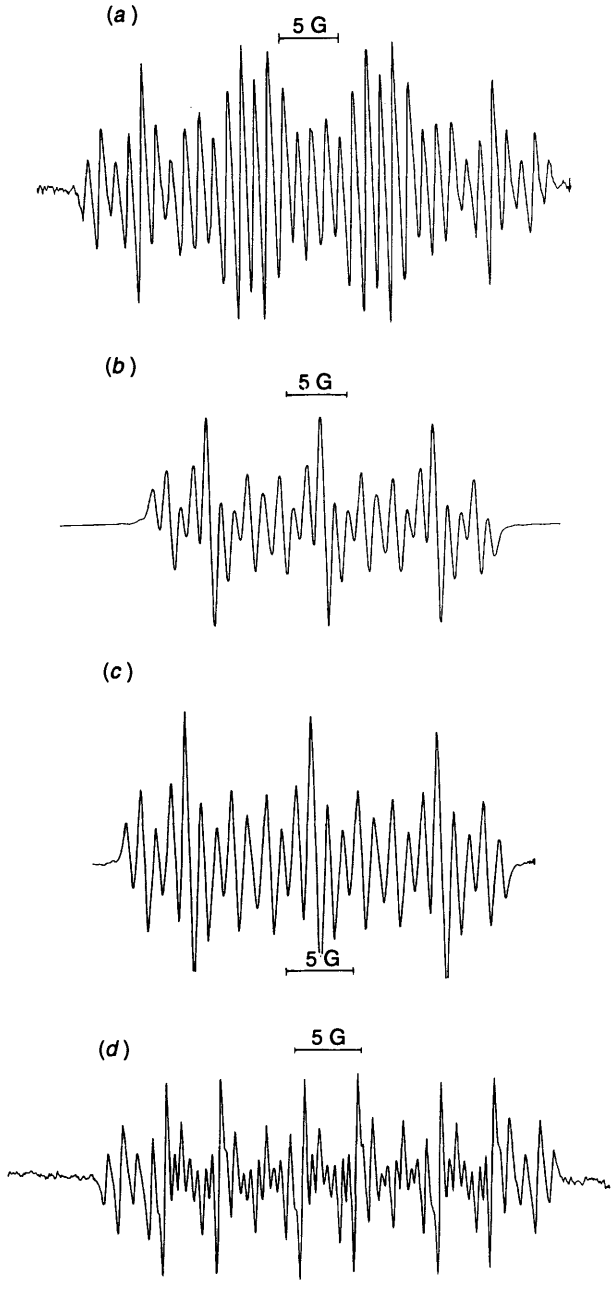

Fig. 1 EPR spectra recorded simultaneously with electrolysis of (*a*) **3** (concentration 1.03 mmol dm^{-3}) attributed to the radical anion, $[F\text{-}C_6H_4\text{-}NO_2]^{\bullet -}$; (*b*) **1** (concentration 1.31 mmol dm^{-3}) attributed to the radical anion, $[Cl\text{-}C_6H_4\text{-}NO_2]^{\bullet -}$; (*c*) **2** (concentration 1.01 mmol dm^{-3}), attributed to the radical anion, $[Br\text{-}C_6H_4\text{-}NO_2]^{\bullet -}$ and (*d*) **4** (concentration 1.00 mmol dm^{-3}) at −1.20 V (*vs.* SCE), attributed to a mixture of the two radical anions, $[C_6H_5\text{-}NO_2]^{\bullet -}$ and $[I\text{-}C_6H_4\text{-}NO_2]^{\bullet -}$

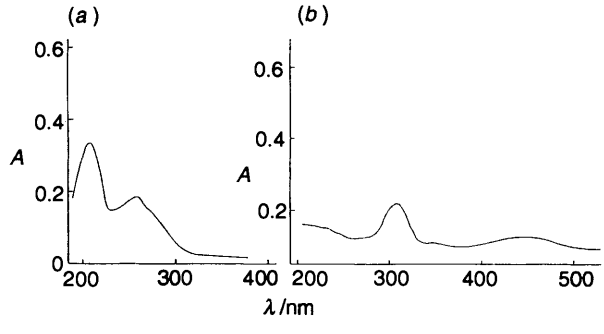

Fig. 2 UV–VIS spectra of (*a*) **3** and (*b*) the radical anion $[F\text{-}C_6H_4\text{-}NO_2]^{\bullet -}$

hydrodynamic voltammetry. Measurement of the steady-state transport limited current as a function of the electrolyte flow rate showed it to obey the Levich equation and this permitted the deduction of a value of 2.1×10^{-5} cm^2 s^{-1} for the diffusion coefficient. Fig. 1(*b*) displays an EPR spectrum recorded simultaneously with the electrolysis of **1** and assigned to the radical anion, [*p*-Cl-C_6H_4-NO_2]$^{\bullet -}$.[10] The variation of the EPR signal intensity with the electrode current and the solution flow rate was used to demonstrate the kinetic stability of the radical anion; eqn. (2) quantitatively described the recorded data.

The UV–VIS spectrum of [*p*-Cl-C_6H_4-NO_2]$^{\bullet -}$ is shown in Fig. 3(*a*). The radical anion spectrum shows bands at λ_{max} = 335 (ε = 25 300) and 488 nm (4090 dm^3 mol^{-1} cm^{-1}). The parent molecule, **1**, shows a longest wavelength absorption band at 270 nm (10 700 dm^3 mol^{-1} cm^{-1}) with negligible absorption above 300 nm, as may be judged from Fig. 3(*b*).

p-*Bromonitrobenzene.* Reduction in acetonitrile–0.1 mol dm^{-3} TBAP followed a one-electron reversible process with a halfwave potential of −1.06 V (*vs.* SCE), as demonstrated by quantitative hydrodynamic voltammetry. Fig. 1(*c*) shows the EPR spectrum obtained from electrolysis of the parent material. The radical anion, [*p*-Br-C_6H_4-NO_2]$^{\bullet -}$, inferred to be generated,[10] was shown to have a lifetime of at least several seconds as inferred from the excellent agreement of the current and flow rate dependence of the EPR signal intensity data with eqn. (2). OTTLE measurements [Fig. 3(*c*)] were used to record the [*p*-Br-C_6H_4-NO_2]$^{\bullet -}$ spectrum which shows bands at λ_{max} = 330 (ε = 31 300) and 470 nm (4210 dm^3 mol^{-1} cm^{-1}). Neutral **2** shows a longer wavelength absorption band at 275 nm (15 000 dm^3 mol^{-1} cm^{-1}) with negligible absorption above 300 nm, as may be noted from Fig. 3(*d*).

Nitrobenzene. This showed a reversible one-electron reduction in acetonitrile with a halfwave potential of −1.11 V (*vs.* SCE). The EPR spectrum of the electrogenerated radical anion, $C_6H_5NO_2]^{\bullet -}$, is shown in Fig. 4. Notice that the spectrum is characterised by six particularly strong lines (marked * in Fig. 4). Fig. 3(*e*) shows the UV–VIS absorption spectrum of the radical anion measured using an OTTLE. Absorption bands are seen at λ_{max} = 325 (ε = 18 100) and 440 nm (3750 dm^3 mol^{-1} cm^{-1}).

p-*Iodonitrobenzene.* This species underwent electro-reduction at −1.07 V (*vs.* SCE) but it was estimated that somewhat more than one electron was passed per molecule reduced. In addition, cyclic voltammetry showed the rapid formation of a new species with a reduction potential close to −1.11 V. This new feature was attributed to the reduction of nitrobenzene formed through the decomposition (in the absence of light) of the initially formed radical anion, [*p*-I-C_6H_4-NO_2]$^{\bullet -}$. This suggestion was confirmed by *in situ* electrochemical EPR which produced the spectrum shown in Fig. 1(*d*); comparison with Fig. 4 shows that the major radical product arising from electrolysis is [C_6H_5-NO_2]$^{\bullet -}$. The mechanism of the electrode process was pursued through examination of the total transport limited current (from reduction of **4** and $C_6H_5NO_2$) at a channel electrode, as a function of electrolyte flow rate. It was hypothesised that the process followed an ECE pathway:

$$p\text{-I-}C_6H_4\text{-}NO_2 + e^- \longrightarrow [p\text{-I-}C_6H_4\text{-}NO_2]^{\bullet -}$$

$$[p\text{-I-}C_6H_4\text{-}NO_2]^{\bullet -} \longrightarrow I^- + {}^{\bullet}C_6H_4NO_2$$

$${}^{\bullet}C_6H_4NO_2 + HS \longrightarrow C_6H_5NO_2 + S^{\bullet}$$

$$C_6H_5NO_2 + e^- \longrightarrow [C_6H_5NO_2]^{\bullet -}$$

For such a mechanism the effective number of electrons transferred in the reaction, N_{eff}, defined as

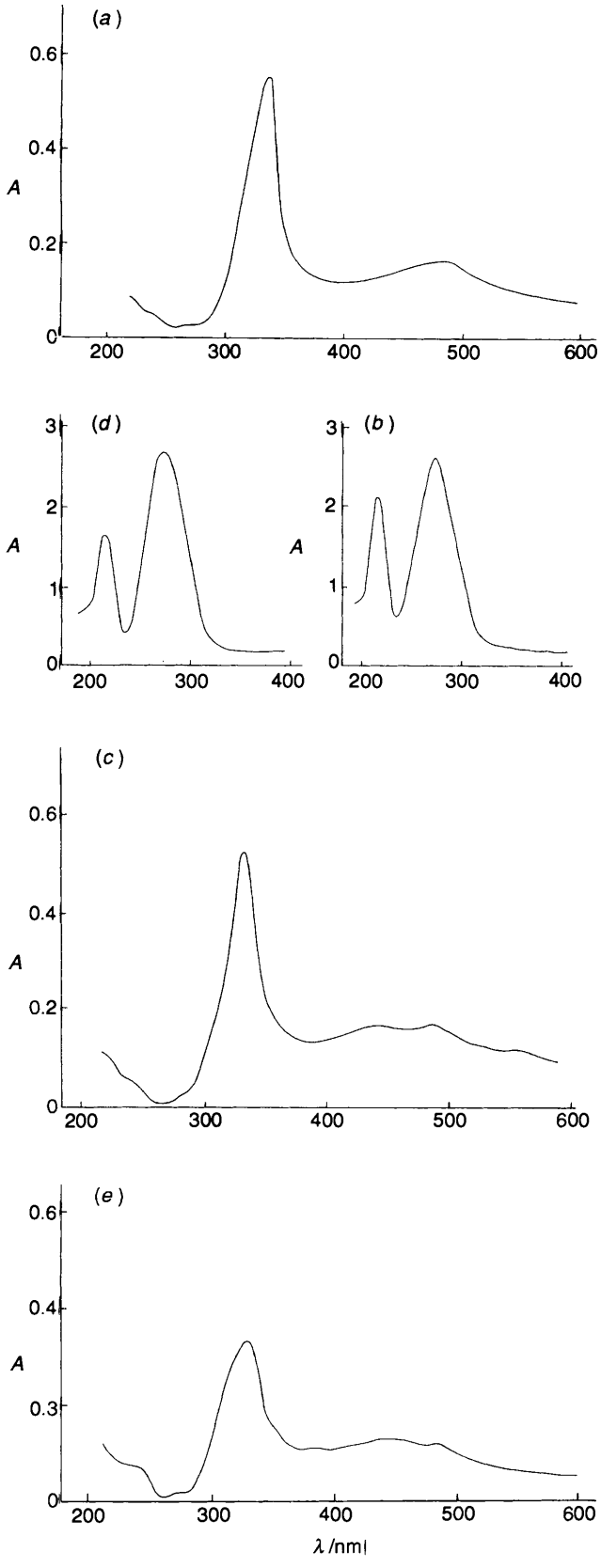

Fig. 3 The UV–VIS spectra of (*a*) the radical anion, [Cl-C_6H_4-NO_2]$^{\bullet -}$, as recorded using an OTTLE,[7] (*b*) **1**, (*c*) the radical anion [Br-C_6H_4-NO_2]$^{\bullet -}$, (*d*) **2** and (*e*) the radical anion [C_6H_5-NO_2]$^{\bullet -}$

$$N_{eff} = \frac{\text{Total limiting current}}{\text{Limiting current for reduction of I-}C_6H_4\text{-}NO_2\text{ only}} \quad (3)$$

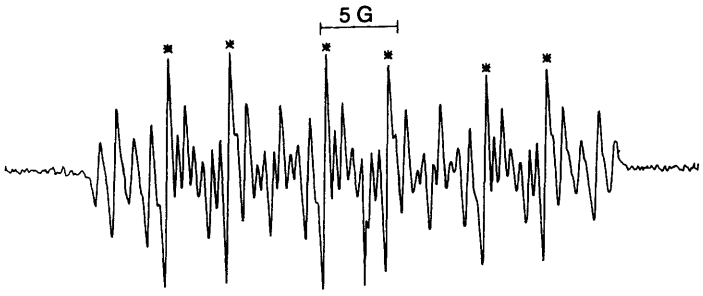

Fig. 4 EPR spectrum of the radical anion $[C_6H_5\text{-}NO_2]^{\bullet -}$

is a unique function of the dimensionless rate constant,

$$K = k\{4h^4x_\theta^2d^2/9V_f^2D\}^{1/3} \quad (4)$$

where k is the rate constant which describes the C-step of the ECE process.[12] A 'working curve' facilitates the analysis of experimental data by relating N_{eff} to K.[12] Limiting current/flow rate measurements were analysed using the above protocol. Specifically current measurements were initially converted into N_{eff} values by assuming a value of $D = 1.84 \times 10^{-5}$ cm^2 s^{-1} for the diffusion coefficient of **4** and employing eqn. (1) to calculate the current due to the reduction of **4** alone. These N_{eff} values were then used to deduce corresponding values of K using the working curve for the ECE mechanism.[12] Last, values of K were plotted against (flow rate)$^{-2/3}$, as suggested by the form of eqn. (4). The resulting plot is shown in Fig. 5 from which it can be seen that an excellent linear dependence is obtained suggesting that the proposed mechanism may likely operate. The slope of the line in Fig. 5 permits the inference of a first order rate constant for the decomposition of the radical anion, $[p\text{-I-}C_6H_4\text{-}NO_2]^{\bullet -}$, of 1.1 s^{-1} which is close to a value reported previously for a slightly different temperature, measured using an independent method.[13] The mechanistic inference is in agreement with all other previous reports[14] on the *p*-iodonitrobenzene system with the exception of one suggestion that iodine atoms, rather than iodide ions, are released.[15] However our experiments showed that no traces of I_2 were detectable with an OTTLE, even under conditions of exhaustive electrolysis for prolonged periods of up to 100 min.

Table 1 summarises all the hyperfine coupling constants derived from the electrochemical EPR experiments reported above.

Photoelectrochemistry.—It is clear that in the case of **4**, electroreduction alone is adequate to accomplish effective cleavage of the weak aryl–halogen bond with release of an iodide anion. We next investigated whether it was possible to induce analogous behaviour in **3**, **1** or **2** by additional photochemical activation following one-electron reduction. The UV–VIS data reported above shows that the radical anions of these three species possess two absorption bands with maxima at wavelengths in the near UV–VIS part of the spectrum, whereas the parent molecules only absorb significantly below 300 nm. The two band maxima are located close to 330 and 470 nm in each case. Accordingly measurements were made in which the potential of the channel electrode was maintained at a value corresponding to the transport limited reduction of the substrate, whilst illuminated by light of wavelengths between 300 and 600 nm. The current flowing as the wavelength was scanned and recorded and any photocurrent noted. The resulting 'action spectra' are shown in Fig. 6 for the three compounds of interest.

Fig. 6 shows that no more than negligible photocurrents were seen at any wavelength in the case of **3**. However, for **1** and **2** appreciable photocurrents were observed. These are discussed in turn below.

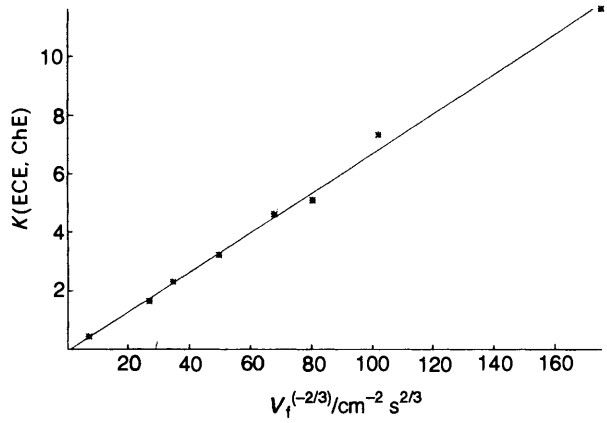

Fig. 5 Analysis of current/flow rate data measured for the reduction of **4** in terms of an ECE mechanism. The channel flow cell used for the measurements had the following geometry: $2h = 0.040$ cm, $w = 0.391$ cm, $d = 0.6$ cm and $x_\theta = 0.401$ cm.

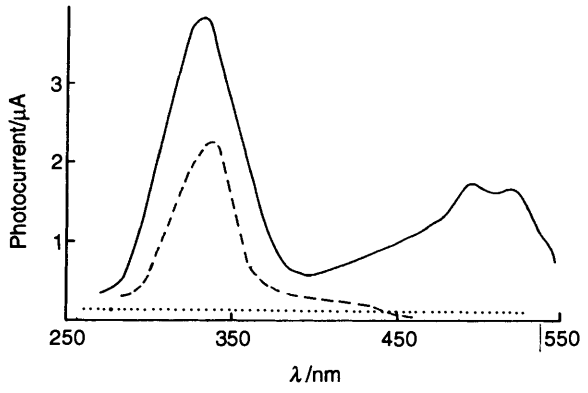

Fig. 6 Action spectra showing the photocurrents flowing as a function of wavelength for **3**, **1** and **2**. Measurements were made using a channel electrode with a flow rate of 1×10^{-3} cm^3 s^{-1} and a concentration of electroactive material of approximately 1.00 mmol dm^{-3} in all three cases: X = (· · ·) F; (– – –) Cl; (——) Br

Table 1 Hyperfine coupling constants[a] (Gauss) for the radical anions investigated

	a_N/G	$a_{o,H}$/G	$a_{m,H}$/G	a_p/G
$C_6H_5\text{-}NO_2^{\bullet -}$	10.3	3.3	1.1	4.0
$\mathbf{1}^{\bullet -}$	9.8	3.5	1.3	—
$\mathbf{2}^{\bullet -}$	9.3	3.4	1.1	—
$\mathbf{3}^{\bullet -}$	10.5	3.5	1.2	8.3

[a] a_N, $a_{o,H}$ and $a_{m,H}$ denote the coupling constants with the nitrogen, *ortho*-hydrogen and *meta*-hydrogen nuclei respectively and a_p corresponds to the *para*-hydrogen in the nitrobenzene radical anion and the fluorine atom in **3**.

p-*Bromonitrobenzene.* Comparison of the action spectrum in Fig. 6 with the UV–VIS absorption spectrum of $[Br\text{-}C_6H_4\text{-}NO_2]^{\bullet -}$ given in Fig. 3 reveals that both the absorption bands (at 330 and 470 nm) stimulate photoelectrochemical activity. We have shown elsewhere[2] that the effect of 330 nm irradiation is the loss of bromide ion *via* the photo-ECE process identified in the Introduction. The nature of the process induced by the 470 nm radiation was analogously examined. *In situ* EPR measurements (Fig. 7) showed that this wavelength of light induced the formation of the nitrobenzene radical anion, as also seen in the case of irradiation using 330 nm. Accordingly the mechanism of the long wavelength process was pursued in terms of a photo-ECE mechanism using photocurrents measured as a function of the electrolyte flow rate at a light intensity of 2 mW cm^{-2}. As for the case of the dark electro-

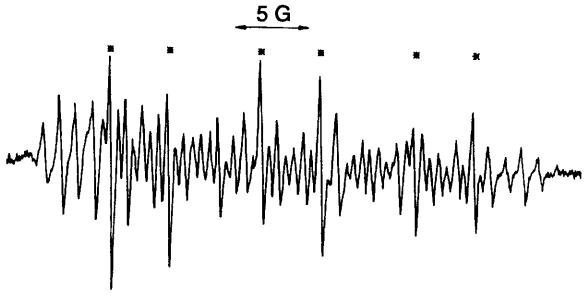

Fig. 7 EPR spectrum recorded for the products of the electrolysis of **2** (concentration 1.01 mmol dm^{-3}) in the presence of light of wavelength 325 nm and attributed to a mixture of the radical anions, $[C_6H_5NO_2]^{\bullet -}$ and $[p\text{-Br-}C_6H_4\text{-}NO_2]^{\bullet -}$

reduction of **4** above, the total current observed can be converted into effective numbers of electrons transferred where now,

$$N_{eff} = \frac{\text{Total limiting current in the light}}{\text{Total limiting current in the dark}} \quad (5)$$

which again is a unique function of the parameter K defined in eqn. (4) where now k describes the rate of the photochemical step giving rise to $C_6H_5NO_2$. The analysis of the photocurrent data proceeds in an equivalent manner to that used in the case of **4**. Fig. 8 shows typical plots resulting from experimental data obtained using two separate concentrations of **2**. Also shown are corresponding results for excitation at 330 nm using the same intensity of light. An excellent linear dependence of K on (flow rate)$^{-2/3}$ is seen for both concentrations confirming that the photo-ECE mechanism defined by steps (a) to (d) operates for light of wavelength 470 nm as well as for 330 nm. The slopes of the lines shown in Fig. 8 permit the inference of a value of 0.052 s^{-1} for the C-step of the ECE process using light of wavelength 470 nm at an intensity of 2 mW cm^{-2}.

p-*Chloronitrobenzene*. Comparison of the action spectrum in Fig. 6 with the UV–VIS absorption spectrum of $[Cl\text{-}C_6H_4\text{-}NO_2]^{\bullet -}$ shown in Fig. 3 reveals that in this case only the short wavelength band (335 nm) is active; excitation of the 488 nm transition produces no photocurrent. The mechanism of dechlorination through the active band was investigated using the flow rate dependence of the steady-state photocurrents. Analysis in terms of N_{eff} and K was pursued as in the case of the **2**, and Fig. 9 again shows a very good linear dependence of K on (flow rate)$^{-2/3}$ confirming that the mechanism is of the photo-ECE type with a first-order rate constant of 0.041 s^{-1} at a light intensity of 2 mW cm^{-2}. Further experiments confirmed the expected linear relationship between the light intensity and the dechlorination rate constant (Fig. 10). This provides further evidence in support of the proposed mechanism; a similar dependence has been reported for **2**.[2]

We next consider the exact nature of steps (b) and (c) in greater detail as probed by experiments in which the photoelectrochemical reductions of **1** (at 335 nm) and **2** (at both 330 and 470 nm) were conducted in the presence of added chloride ion in the former case or added bromide ion in the latter case. Experiments were conducted using constant ionic strength mixtures (=0.10 mol dm^{-3}) of TBAP and either TBAC or TBAB such that the concentration of the halide ion, X^- (X = Cl or Br), varied in the range $0 < [X^-]/\text{mol dm}^{-3} < 0.10$. In all three cases the addition of halide was found to diminish the magnitude of the observed steady-state photocurrents but the dependence of the latter on the solution flow rate confirmed that an ECE mechanism still operated in the presence of X^-. It was therefore possible to deduce how the rate constant, k, for the C-step varied with $[X^-]$. This data was considered in the light of the ECE mechanism given above with the inclusion of the additional possibility that step (b) is reversible:

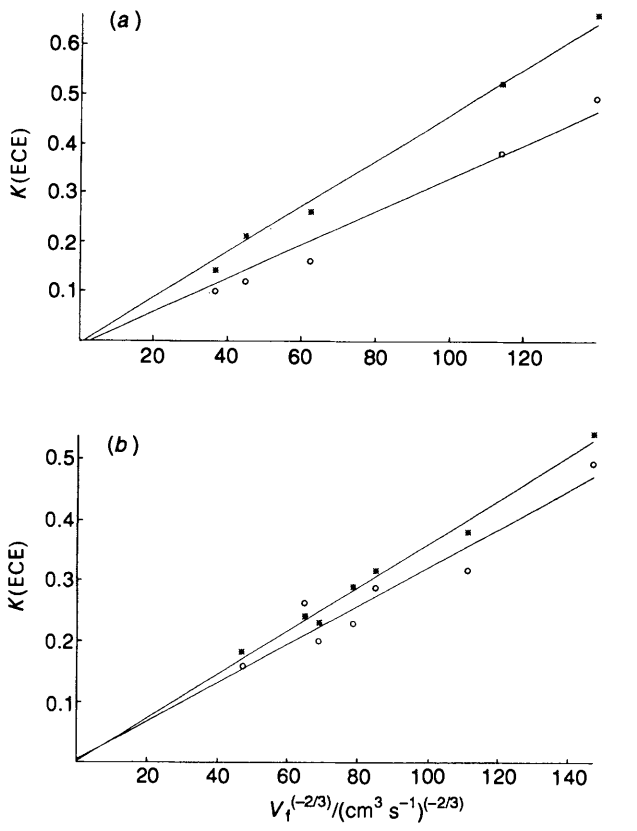

Fig. 8 Analysis of photocurrent/flow rate data measured using light of wavelengths 330 and 470 nm and intensity 2 mW cm^{-2} for concentrations of **2** of (*a*) 0.53 and (*b*) 1.05 mmol dm^{-3}. The channel flow cell used for the measurements had the following geometry: $2h$ = 0.044 cm, w = 0.367 cm, d = 0.6 cm and x_0 = 0.412 cm. λ = (*) 330; (○) 470 nm.

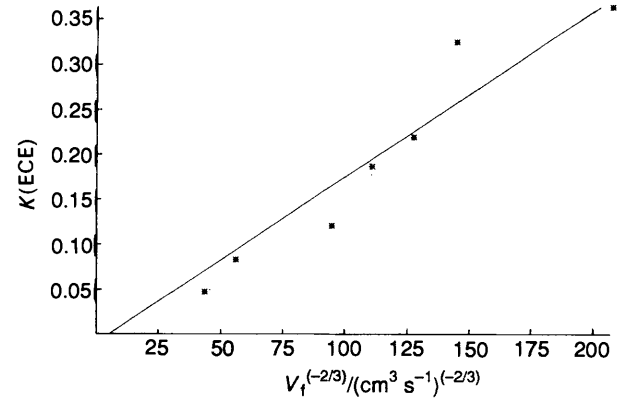

Fig. 9 Analysis of photocurrent/flow rate data measured using light of wavelength 335 nm and intensity 2 mW cm^{-2} for **1** of 0.99 mmol dm^{-3}. The channel flow cell used for the measurements had the following geometry: $2h$ = 0.046 cm, w = 0.367 cm, d = 0.6 cm and x_0 = 0.412 cm.

$$X^- + {}^{\bullet}C_6H_4NO_2 \longrightarrow [p\text{-X-}C_6H_4NO_2]^{\bullet -} \quad (f)$$

Applying the steady-state hypothesis to ${}^{\bullet}C_6H_4NO_2$ gives eqn. (6), where $k_{(b)}$, $k_{(c)}$ and $k_{(f)}$ are the rate constants for the

$$k \propto \text{Int.}k_{(b)}/\{k_{(c)} + k_{(f)}[X^-]\} \quad (6)$$

steps (b), (c) and (f), respectively and Int denotes the intensity of incident light on the ChE.

Eqn. (6) suggests first that k should be directly proportional to the light intensity which has been shown to be the case for **1** above and has been reported elsewhere [2] for **2**. Secondly, eqn. (6)

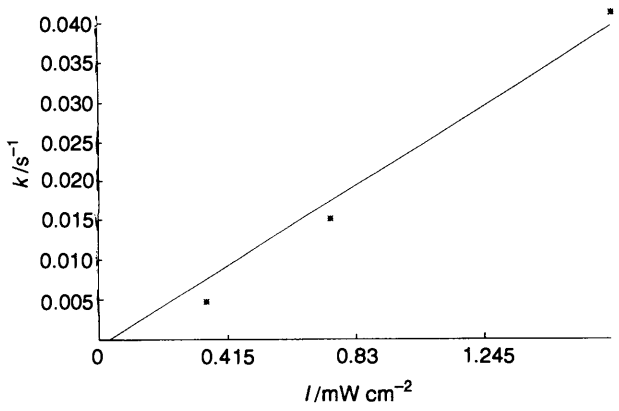

Fig. 10 The rate constant for the C-step of the ECE process shown to describe the dechlorination of $[p\text{-Cl-C}_6\text{H}_4\text{-NO}_2]^{\bullet -}$ (0.51 mmol dm^{-3}) by light of wavelength 335 nm, depends linearly on the light intensity incident on the electrode surface

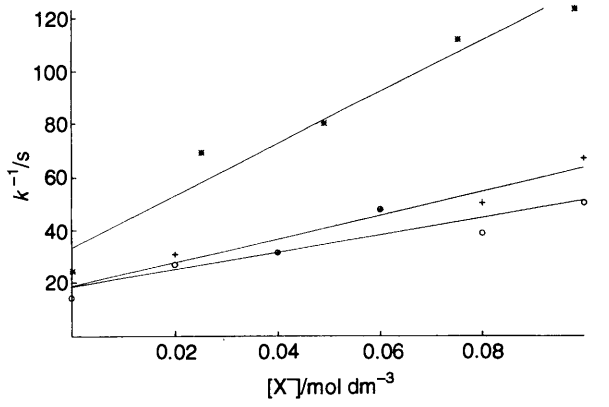

Fig. 11 Analysis of the dependence of the ECE rate constant, k, measured at a light intensity of 2 mW cm^{-2} on $[X^-]$ according to eqn. (6) for **1** [335 nm (*)] and **2** [330 (○) and 470 (+) nm]

implies that a plot of k^{-1} against $[X^-]$ should be linear. The latter is shown in Fig. 11 which suggests the veracity of eqn. (5) and the mechanism on which it is based. Note that this implies that both steps (c) and (f) are kinetically significant in controlling the fate of $^{\bullet}C_6H_4NO_2$; step (b) is not a pre-equilibrium preceding step (c). Analysis of lines in Fig. 11 shows, by comparison of the slope and intercepts of each of the lines, that the ratio $k_{(f)}/k_{(c)}$ has the following values: 40.1 (Cl, 335), 22.9 (Br, 330) and 23.1 mol dm^{-3} (Br, 470 nm). The fact that the two values measured at different wavelengths for **2** are, within experimental error, identical lends yet further very strong evidence for the proposed mechanistic scheme.

Finally we note that since $k_{(c)}$ is expected to be independent of the particular *p*-halonitrobenzene used to generate the $^{\bullet}C_6H_5NO_2$ radical, the relative nucleophilicities of Br^- and Cl^- towards this aryl radical may be estimated from the $k_{(f)}/k_{(c)}$ ratios given above:

$$\frac{k_{(f)}(Cl^-)}{k_{(f)}(Br^-)} = \frac{40.1}{23.0} = 1.74 \qquad (7)$$

We note that this value is close to the ratio of the diffusion coefficients of the two anions, $D(Cl^-)/D(Br^-) = 1.57$,[16] which possibly hints that step (f) is close to diffusion controlled.

Discussion

Compounds **1** and **2** behave differently under conditions of photoelectrochemical reduction. In the former only excitation

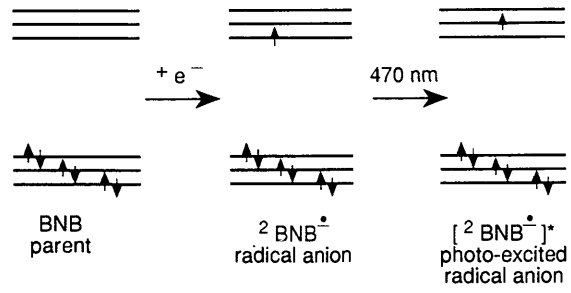

Fig. 12 Schematic diagram showing that excitation at 470 nm leads to a doublet excited state of the radical anion $[p\text{-Br-C}_6\text{H}_4\text{-NO}_2]^{\bullet -}$

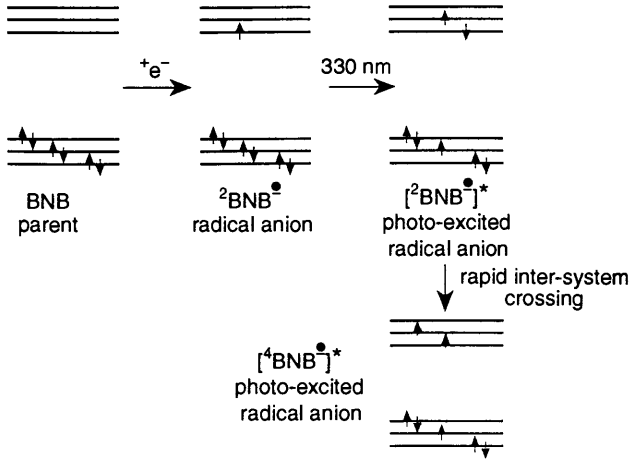

Fig. 13 Schematic diagram showing that excitation at 330 nm may lead to an excited state of the radical anion $[p\text{-Br-C}_6\text{H}_4\text{-NO}_2]^{\bullet}$ which is a quartet

of the short wavelength transition at 335 nm is effective towards inducing halide loss from the radical anion, whereas in the latter both short (330 nm) and long (470 nm) wavelength excitations of $[Br\text{-C}_6\text{H}_4\text{-NO}_2]^{\bullet -}$ are successful in causing bromide expulsion. We suggest that the failure of long wave (488 nm) radiation to accomplish dehalogenation in **1** reflects the strength of the C–Cl bond (ΔH = 396 kJ mol^{-1})[17] relative to that of the C–Br bond (ΔH = 332 kJ mol^{-1})[17] where the corresponding band is particularly effective.

We next consider the relative efficiency of excitation at 470 nm, as compared to 330 nm, towards the rate of bromide expulsion from $[Br\text{-C}_6\text{H}_4\text{-NO}_2]^{\bullet -}$. Examination of Fig. 6 shows that the magnitude of the photocurrents associated with the 470 nm band are of comparable intensity to those caused by 330 nm radiation from the same source despite the fact that the extinction coefficient of the former is some 7.5 times weaker than the latter, indicating the more efficient bromide release from the excited state accessed by the lower energy radiation. This faster reaction (by a factor of 5.6 per photon absorbed) *via* the lower energy excited state in **2** is reminiscent of the behaviour reported for the halo-anthraquinones.[5,6] A possible explanation arises from consideration of the likely electronic structure of the two excited states. Since the long wavelength absorption can be assigned as a π^* to π^* transition,[18] the resulting excited state necessarily has doublet character. In contrast, the 330 nm band is likely to involve the excitation of a π electron which may ultimately result in the formation of an excited quartet state through rapid intersystem crossing. The two cases are shown in Figs. 12 and 13. The loss of closed shell species such as halide ions from the latter is a spin forbidden process:

$$^4(p\text{-Br-C}_6\text{H}_4\text{-NO}_2^{\bullet -})^* \longrightarrow Br^- + {}^2(^{\bullet}C_6H_4NO_2)$$

However, it is spin allowed from doublet states:

$$^2(p\text{-Br-}C_6H_4\text{-}NO_2^{\bullet -})^* \longrightarrow Br^- + {}^2(^\bullet C_6H_4NO_2)$$

The contrasting behaviour observed may therefore reflect the operation of spin conservation rules.

Acknowledgements

We thank NERC for a studentship for R. A. W. D. and SERC for financial support (Grant Number GR/H99288). We thank Judy Hirst for experimental assistance.

References

1 R. G. Compton, R. A. W. Dryfe and A. C. Fisher, *J. Electroanal. Chem.*, 1993, **361**, 275.
2 R. G. Compton and R. A. W. Dryfe, *J. Electroanal. Chem.*, in the press.
3 R. G. Compton, R. Barghout, J. C. Eklund and A. C. Fisher, *Electroanalysis*, 1994, **6**, 45.
4 R. G. Compton, R. Barghout, J. C. Eklund, A. C. Fisher, A. M. Bond and R. Colton, *J. Phys. Chem.*, 1993, **97**, 1661.
5 R. G. Compton, R. G. Wellington, A. C. Fisher, D. Bethell and P. Lederer, *J. Phys. Chem.*, 1991, **95**, 4749.
6 R. G. Compton, B. A. Coles, M. B. G. Pilkington and D. Bethell, *J. Chem. Soc., Faraday Trans.*, 1990, **86**, 663.
7 M. B. G. Pilkington, B. A. Coles and R. G. Compton, *Anal. Chem.*, 1989, **61**, 1787.
8 L. Holleck and D. Becher, *J. Electroanal. Chem.*, 1962, **4**, 321; T. Osa and T. Kuwana, *J. Electroanal. Chem.*, 1969, **22**, 389; J. G. Lawless and M. D. Hawley, *J. Electroanal. Chem.*, 1969, **21**, 365; 1969, **23**, Appendix 1.
9 V. G. Levich, *Physicochemical Hydrodynamics*, Prentice-Hall, New Jersey, 1962.
10 D. H. Geske and A. H. Maki, *J. Am. Chem. Soc.*, 1960, **82**, 2671; 1961, **83**, 1852; P. B. Ayscough, F. P. Sargent and R. Wilson, *J. Chem. Soc.*, 1963, 5418; P. L. Kolker and W. A. Waters, *J. Chem. Soc.*, 1964, 1136; J. Q. Chambers, T. Layloff and R. N. Adams, *J. Phys. Chem.*, 1964, **68**, 661.
11 R. G. Compton, R. A. W. Dryfe and J. C. Eklund, *Res. Chem. Kinet.*, 1993, **1**, 246.
12 R. G. Compton, M. B. G. Pilkington and G. M. Stearn, *J. Chem. Soc., Faraday Trans.*, 1988, **84**, 2155.
13 R. F. Nelson, A. K. Carpenter and E. T. Seo, *J. Electrochem. Soc.*, 1973, **120**, 207.
14 T. Kitagawa, T. P. Layloff and R. N. Adams, *Anal. Chem.*, 1963, **35**, 1086; T. Fujinaga, Y. Deguchi and K. Umemoto, *Bull. Chem. Soc. Jpn.*, 1964, **37**, 822; 1973, **46**, 2716; V. D. Parker, *Acta Chem. Scand., Ser. B*, 1981, **35**, 655.
15 I. M. Sosonkin and G. N. Strogov, *Sov. Electrochem.*, 1984, **20**, 453.
16 T. Iwasta and M. L. Giordano, *Electrochim. Acta* 1969, **14**, 1045; A. I. Popov and D. H. Geske, *J. Am. Chem. Soc.*, 1958, **80**, 5346.
17 R. S. Davidson, J. W. Goodin and G. Kemp, *Adv. Phys. Org. Chem.*, 1984, **20**, 191.
18 A. Fulton, *Aust. J. Chem.*, 1968, **21**, 2847.

Paper 4/00486H
Received 26*th January* 1994
Accepted 31*st March* 1994